Effect of macromolecular polymer structures on drag reduction in a turbulent channel flow

K. Kim
Department of Naval Architecture and Marine Engineering, University of Michigan, Ann Arbor, Michigan 48109-2145

M. T. Islam
Department of Naval Architecture and Marine Engineering, University of Michigan, Ann Arbor, Michigan 48109-2145
and Department of Chemical Engineering, University of Michigan, Ann Arbor, Michigan 48109-2145

X. Shen and A. I. Sirviente[a)]
Department of Naval Architecture and Marine Engineering, University of Michigan, Ann Arbor, Michigan 48109-2145

M. J. Solomon
Department of Chemical Engineering, University of Michigan, Ann Arbor, Michigan 48109-2145

(Received 23 October 2003; accepted 21 July 2004; published online 6 October 2004)

This paper presents the influence of injected polymer solutions on turbulence in fully developed channel flows. In particular, it investigates the impact of concentration and mixing of the polymer solution on drag reduction. It is observed, via flow visualization and birefringence measurements, that for large injection concentrations macromolecular polymer structures exist in the flow. They are found to be mostly located in the neighborhood of the channel centerline. Laser Doppler velocimetry was used to characterize the mean and turbulent flow with and without the presence of macromolecular polymer structures. © *2004 American Institute of Physics*.
[DOI: 10.1063/1.1790731]

I. INTRODUCTION

Engineers have been interested in understanding polymer solution effects on turbulent friction mechanisms since Toms[1] first published his drag reduction data. The potential applications of friction reducing polymers are ample. They are currently being used for transport of oil in pipelines (Trans-Alaska Pipeline), for sewer and drainage systems, and, in fire-fighting equipment, among others. The potential of using polymers as drag reduction agents for ships or submersibles is significant, but to date an economically feasible approach for their implementation in the marine industry has not been found. Interest also exists in the biomedical industry for drag reducing agents to treat or prevent blood circulation problems. Sellin *et al.*[2] present a detailed review of present applications of such drag reduction agents.

The phenomenon of polymer drag reduction involves disciplines as diverse as hydrodynamics, rheology, and polymer chemistry among others. It is this diversity of areas that makes the problem interesting and challenging. Generally, the studies found in the literature fall in one of the following two categories. The first category is aimed at characterizing the changes in the mean and turbulent flow due to the presence of polymers; and the second is focused on understanding the mechanism of action of the polymer molecules in solution. Most of the work performed under the first category was done under the assumption that polymer molecules in dilute solutions exist as isolated random coils. The work of Dunlop and Cox,[3] on the other hand, showed that molecular aggregates in solutions of poly(ethylene oxide) (PEO), polyacrylamide (PAM), and others are fairly common. They characterized aggregates as "any group of polymer molecules bound together by physical forces." Their study also provides a detailed review of the polymer chemistry literature showing many studies discussing various methods for polymer aggregate detection in different solvents. In this study, the term "aggregate" is used to refer to polymer structures of ionic polymers, where ionic and hydrogen bonds are expected to be mainly responsible for the cluster formation. The term "entanglement," on the other hand, is used to refer to polymer structures of nonionic polymers since they are expected to be maintained mainly by mechanical bonds.

In this study, the drag reduction additive of choice is a PAM. Today, PAM and PEO are probably the most widely used water-soluble polymers in commercial applications. Both are linear, flexible molecules, which can be obtained in a wide range of molecular weights. Studies indicate that PAM is able to endure shear degradation better than PEO.[4] The work of Richardson[5] shows a fibrilar structure with a high degree of complexity for a very dilute aqueous solution (10 ppm) of polyacrylamide examined by scanning electron microscopy. Liberatore *et al.*[6] report on the production of structures in polyacrylamide solutions at high shears in a Couette device. The work of Boyadjian *et al.*[7,8] showed higher level of such formations with increasing molecular weight and ionic character of the polymer solution. It seems

[a)]Author to whom correspondence should be addressed. Electronic mail: asirv@engin.umich.edu

that it is reasonable to expect a certain level of interaction between polymer chains even in very dilute polymer solutions.

To date, there are many proposed mechanisms to explain the phenomenon of drag reduction by injection of very dilute polymer solutions. Lumley[9] proposed that the mechanism for drag reduction was an increased viscosity near the wall, caused by elongational deformation of the molecules by the turbulence. Arguments based on the kinetics of the molecules have been recently introduced by De Gennes[10] and O'Shaughnessy *et al.*[11] among others. Despite decades of work in this area, there is not yet a universally accepted mechanism. Questions have been posed as to whether or not polymer drag reduction is a phenomenon taking place exclusively in the near wall region. Some experimental results seem to indicate that concentrated polymer solutions injected into the centerline of a pipe can result in drag reduction even before the polymer has reached the wall.[12] Past investigations in channels or pipes with injection of very dilute polymer solutions show that for low drag reduction percentages, the behavior of most turbulence characteristics is very similar to Newtonian flows. On the other hand, for large drag reduction percentages important differences can be found for the mean and turbulence quantities with respect to the corresponding Newtonian flow. Laser Doppler velocimetry measurements of mean and turbulent characteristics of polymer flows show that the presence of polymers translates into an increase in the thickness of the buffer zone of the turbulent boundary layer. The larger the drag reduction, more the change observed to the slope of the logarithmic law, and more the drastic modification of the turbulence quantities (i.e., the work by Rieschman and Tiederman,[13] Wei and Willmarth,[14] Den Toonder *et al.*[15] among others). For very large percentages of drag reduction, the polymers seem to inhibit both streamwise and transverse velocity fluctuations and, consequently, their correlation.[16] In addition, the flow also shows negligible values for the Reynolds stress in some cases.[17,18] Visualization of the coherent turbulent structures present in a turbulent boundary layer when polymer is injected,[19–21] as well as results from burst detection algorithms[22,23] indicate larger streak spacing and reduction of the bursting rate. The latter is directly related to the reduction of the Reynolds stress. However, even when the Reynolds stress is practically zero across the flow, there is still a substantial amount of drag present which should in some form be linked to the existence of turbulent boundary layer coherent structures, even though modified. In the recent study of Gampert *et al.*[24] laser Doppler velocimetry (LDV) and birefringence measurements were gathered to determine the extension and orientation of aqueous solutions of PAM and Xanthan gum in a square channel.

Results from direct numerical simulation (DNS) of polymer flows in turbulent channels have also revealed many of the changes to the turbulence statistics mentioned above (see the work of Sureshkumar *et al.*[25] and Dimitropoulos *et al.*[26] among others). On the other hand more recent DNS studies of polymer flows show that polymer drag reduction can take place in homogenous turbulent flows.[27] The results of De Angelis *et al.*[28] and Benzi *et al.*[27] argue that the mechanism of drag reduction is mainly linked with the modification of the dynamics of the large scales in the flow instead of the small dissipative scales as it has been traditionally accepted.

Recently, the studies of Vlachogiannis and Hanratty[29] and Vlachogiannis *et al.*[30] report experiments dealing with heterogeneous polymer solutions. In their experiments the presence of polymer filaments was found right after the preparation of the polymer solution and prior to its injection in the channel. Their work involves the use of a hydrolyzed polyacrylamide, whose ability to aggregate increases due to its ionic character.[7,8]

In this study, the influence of concentration and mixing on drag reduction in a turbulent channel flow with polymer injection is reported. To search for the presence of large-scale concentration inhomogeneity in the channel flow studies, *in situ* optical measurements of birefringence, dichroism, and turbidity were performed. Birefringence, anisotropy in the real component of the refractive index tensor, is related to orientation and stretching of polymer molecules. Dichroism, anisotropy in the imaginary component of the refractive index tensor, is related to the scattering of light by oriented objects. Turbidity is the attenuation of light due to scattering or absorption. These three optical measurements are complementary in nature—each probes a different aspect of the response of polymer molecules in the flow. The measurements are sensitive to the behavior of polymer molecules over the beam path, which in this study is propagated along the neutral axis of the flow. Spatial resolution in the gradient direction is obtained by traversing the optical device along the width of the flow channel. As a result of these measurements and laser induced fluorescence (LIF) visualization of the flow, it is observed that for large injection concentrations macromolecular polymer structures exist in the flow and are mostly located in the centerline region. Laser Doppler velocimeter measurements of mean velocity and turbulence are compared for polymer solutions with and without those structures. Their corresponding drag-reducing abilities are found to be very different.

II. EXPERIMENTAL APPARATUS AND PROCEDURES

A. Water channel

The recirculating channel used in this experimental study is located at the Marine Hydro-laboratory of the Naval Architecture and Marine Engineering Department at the University of Michigan. The channel is shown schematically in Fig. 1. In this experimental facility, the flow is driven by a $0.076\ m^3/s$ centrifugal pump into a 5.99 cm wide by 59.94 cm high and 6.35 m long channel test section. The bulk velocity in the test section can be up to 2.11 m/s, leading to a Reynolds number based on the channel's width up to 1.26×10^5.

Settling chambers are located at each end of the test section. They are similar in design; both are 120 cm long, 67 cm wide, and 60 cm high at the edges and 65 cm high at the center. Water exits the upstream settling chamber through a 61 cm long one-dimensional planar contraction and enters the downstream settling chamber through an identically shaped expansion. Both settling chambers and the planar

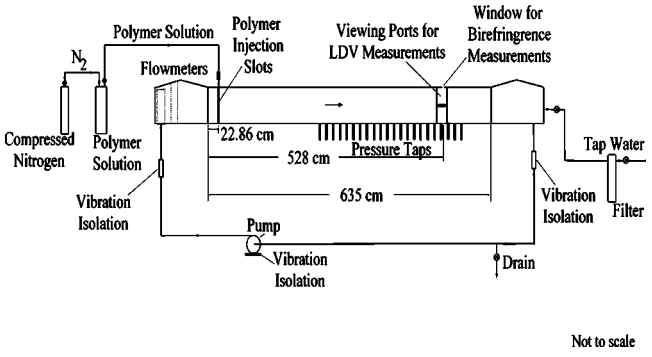

FIG. 1. Schematic of the channel.

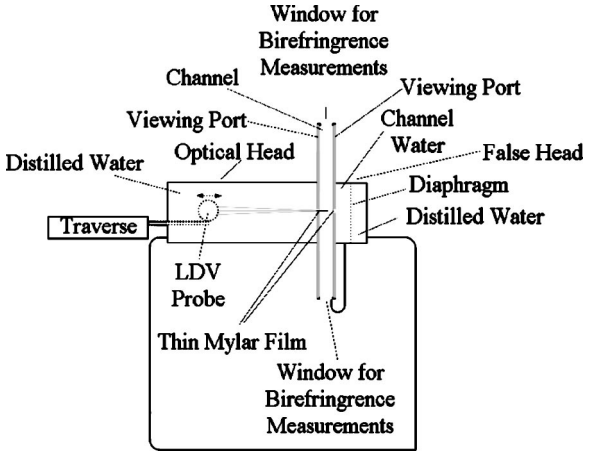

FIG. 2. Schematic of the channel's measurement station (front view).

contraction and expansion are made of 2 cm thick PVC sheets. Conditioning of the flow is done with two stainless steel screens, placed in the upstream settling chamber, spaced 13 cm apart. The test section geometry was designed so that the flow would approximate that between two infinite parallel plates, be fully developed at the measurement station, and have a homogeneous polymer concentration at the test section. To that end the test section aspect ratio (height/width) was chosen to be 10, since for channel flow to approximate flow between two infinite flat plates, the aspect ratio must be at least 7.[31] The measurement station is located 88.5 channel widths downstream of the test section entrance and 84.4 channel widths from the injection slot. The positioning of the measuring station was selected by following the recommendations made in the literature. The study of Comte-Bellot[32] showed that the fully developed regime, where all statistical moments are independent of the downstream distance, is established by about 60 channel heights (corresponding to widths in the present design) downstream of the inlet. She measured the skewness and flatness factors to further prove that a fully developed regime had been established by then, by showing negligible changes for both. The studies of Wei[33] and Velazquez[34] among others have shown that the flow is fully developed well before 80 channel widths. Walker *et al.*[35] showed that the drag reduction in channel flow becomes constant within 30 channel widths from the polymer injection station.

The measurement station is located 5.28 m downstream of the test section entrance. Twenty-one equally spaced pressure taps (0.31 cm in diameter) are located on one of the test section walls to monitor the pressure gradient. They are located every 15.24 cm from 2.51 m to 5.72 m downstream of the test section entrance. The polymer injection slots are located 22.86 cm downstream of the test section entrance on both sides of the channel. They are 0.25 cm wide, 59.94 cm high and are inclined at an angle of 25° to the wall. The width and angle of the injection slots were chosen based on past data reported in the literature.[35] A pneumatic system drives the polymer solution from storage tanks to the injection slots. The polymer solution is stored in a 16-gallon pressure tank. Compressed nitrogen forces the polymer solution from the pressure tank into the injection slots. A needle valve with a micrometer handle located at the exit of the nitrogen cylinder regulates the flow rate; flow meters near each injection slot are used to monitor the flow rate. The injection concentration is denoted as C_i in this study, while the corresponding mixed concentration at the test section is C_h.

Special optical access is provided at the measurement station. Quartz windows 0.8 cm thick by 2.5 cm wide by 8 cm long replace the acrylic directly above and below the measurement station to provide access for the optical birefringence measurements. Viewing ports, 25 cm long by 60 cm high and 2 cm thick brass plates replace the acrylic on both side walls at the measurement station. Each viewing port has a slot 2.54 cm high by 15.24 cm long machined through its center and the inside of these slots are covered with 0.005 cm thick, clear Mylar film. Two small water tanks on both sides of the channel are used to balance the pressure exerted on the Mylar film by the water in the test section. The water levels in the tanks are adjusted so that the pressure exerted on the Mylar film by the water in the tanks matches the pressure exerted by the water in the test section. This hydrostatic adjustment is accomplished using Tygon tubing to connect the corresponding tanks. A similar design was used by Wei and Willmarth.[36] A schematic diagram of the measurement station is shown in Fig. 2.

The temperature of the water in the channel and in the injected polymer solution is monitored to ensure that it remains constant throughout the experiment. The channel water, polymer solution, and room temperatures are measured using type K thermocouples with 0.1 °C resolution.

B. Experimental instrumentation

1. Mean velocity and turbulence measurements

Measurements of the velocity components and turbulence intensities were made in this study with a laser Doppler velocimeter. The LDV system used makes use of a 5 W Coherent Innova 70 C argon-ion laser. The system is based on the dual-beam method, i.e., on comparison of the frequencies of light scattered in the same direction from two different illuminating beams. Consequently, the laser beam is split into three different color beam pairs, a 488 nm blue, a 514 nm green, and a 476.5 nm violet (TSI-ColorBurst Mo. 9201). Measurements of negative velocities are possible by shifting the frequency of one beam in each pair by 40 MHz by means

of acousto-optic Bragg cells. Fiber optic cables carried the laser light for each of the beams to the underwater probe. A custom-made, single, waterproof three-component laser LDV probe has been made by TSI, Inc. In this study only two-dimensional measurements are reported. The LDV probe is placed in the optical head so that the laser beams enter the test section through the Mylar film. This aids reducing refraction and consequently improving the signal to noise ratio of the LDV measurements. At the end of each fiber there is a collimating, assembly that allows for steering, collimation, and focusing of each of the beams. The six beams are crossed at the same point and aligned with the receiving fiber. The fringe spacing for the green, blue, and violet systems is 3.11, 3.0, and 2.91 μm, respectively. Each beam pair forms an effective measuring volume approximately 83 μm in diameter with a length-to-diameter ratio of approximately 2.5:1. The LDV system is operated in the coincidence mode so that only simultaneous measurements of all velocity components are taken. The coincidence window size is determined by the fluid transit time at each point to achieve optimal Reynolds stress measurements.[37] The receiving optic module is located in the center of the probe and composed of a receiving optic module. The channel is seeded with titanium dioxide of rutile particles in crystalline form of 3 μm in diameter. Scattered light is collected in the backscatter mode, color filtered and focused onto individual photomultipliers (TSI-ColorLink Mo. 9230). The signals so generated are down-mixed to yield an effective shift frequency of 200 KHz on all colors. The signals from the frequency downmixers are fed onto a TSI IFA 655 digital burst correlator signal processor that determines and records the frequency of the Doppler bursts from all channels after bandpass filtering the signals. The correlation processor is digitally interfaced to a Pentium II PC to process the signals.

A one-axis traverse system from Velmex, Inc. (Velmex model No. MB4009K2J-S4 with a Velmex VP9000 controller), mounted on top of the optical head moves the LDV probe so that measurements can be made across the entire width of the test section. The traverse moves 2.0 mm/revolution and the controller has 400 steps/revolution, which gives accuracy for the positioning of the measuring volume of 5 μm. The measuring volume was initially checked to move parallel to the channel bottom.

2. Postprocessing of LDV measurements

Measurements were taken at 60 locations between walls. The sampling rate was around 50 Hz in the near wall region and reached up to 600 Hz in the centerline. At each measuring position up to 50 000 velocity triplets were collected. These data were then number averaged and refined. Realizations that were more than three standard deviations away from the mean on any component were removed. The velocities were then transformed into the adequate coordinate system, and the corresponding statistics calculated. Corrections for velocity bias were performed with the transit time weight method. This correction is based on the inverse proportionality of the burst time to the magnitude of the velocity vector. TSI's FIND software was used to process the signals.

The data sampled was also contaminated with noise from different components of the LDV system, such as photomultipliers, frequency downmixers, and signal processors. This electronic noise can be determined from the power spectrum of the corresponding fluctuating velocity and its signature is evident in the high frequency region of the spectrum. It is assumed that the noise is white and uncorrelated with the true signals. If a plateau of slope is observed in the high frequency region of the spectrum, the magnitude of the noise is determined by the area of such plateau extended to all frequencies (noise energy), or by a trial and error process to account for the changes in slope. Corrections to account for this electronic noise were made by subtracting the energy of the noise from the energy at all frequencies to determine the corrected spectrum.[38,39] The corrected spectrum is then integrated to obtain the mean square of the fluctuating velocity components. The Reynolds stress could be corrected in the same manner.[40] But this correction should take the noise in the streamwise and normal fluctuation velocity components into account. Since the correlation of the noise in the two fluctuation velocities is unknown, this correction may lead to inaccurate results, and therefore, is not included. The corrections for the turbulence intensities result in

$$\overline{(u_i^t)^2} = \overline{(u_i^m)^2} - \overline{(u_i^n)^2}, \tag{1}$$

where u_i^m, u_i^t, and u_i^n denote the measured and true signal and the noise contribution, respectively.

Measurements of turbulence intensity with oversized probes can also be a source of error[41–43] since a probe essentially integrates over the sensing element's length, area, or volume. Consequently, large-amplitude signals from small structures of dimensions smaller than the sensor size are attenuated. In this study for the Reynolds number 5.6×10^4 (based on the mean centerline velocity and the channel width) the dimensionless LDV measuring volume is approximately three viscous lengths. Corrections for the mean velocities and the mean square of the velocity fluctuations are also made to account for the size of the measuring volume following Durst *et al.*[44] The correction for the turbulent intensities is

$$\overline{(u_i^t)^2} = \overline{(u_i^m)^2} - \frac{d_{mv}^2}{16}\left(\frac{dU}{dy}\right)^2, \tag{2}$$

where $d_{mv}=200$ μm is the diameter of the measurement volume.

The sizes of the ensembles used were up to 50 000 samples to reduce the errors inherent in the calculation of the corresponding statistics. Such ensemble sizes for water flows and polymer flows translated into an uncertainty of 1% on mean velocity, less than 1% on normal stresses and less than 3% on the shear stresses.

3. Birefringence, dichroism, and turbidity apparatus

The apparatus, shown schematically in Fig. 3, includes the optical system, a mechanism to traverse the optics along the width of the channel, and an automated data acquisition system. The optical system was configurable to allow the *in*

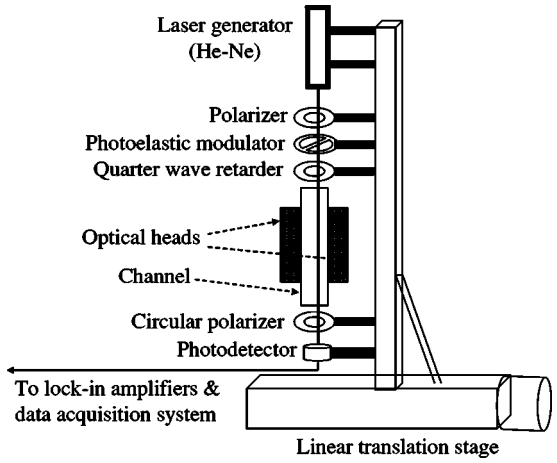

FIG. 3. Schematic diagram of the optical train for birefringence, dichroism, and turbidity measurements.

situ measurement of birefringence, dichroism or turbidity in the channel.

Birefringence. The optical system is based upon a phase modulated polarization scheme described by Fuller.[45] It consists of a helium-neon laser (L), linear polarizer (LP), quarter wave retarder (Q), photoelastic modulator (PEM), and a circular polarizer (CP) configured as follows: $LP_{@90°}PEM_{@45°}Q_{@0°}S_{\delta@\chi°}CP$ (Fig. 3). All orientation angle subscripts are defined relative to the direction of flow. Here S represents a polymer sample with birefringence retardation δ and orientation angle χ. The retardation $\delta=\Delta n(2\pi d)/\lambda$, where Δn is the sample birefringence, d is the path length in the neutral direction, and λ is the wavelength of the laser light. In the PEM, the electric field along the slow axis (45° axis) is retarded relative to its value along the fast axis, which is perpendicular to the slow axis, by an amount δ_{PEM} that varies in a sinusoidal fashion $[\delta_{\mathrm{PEM}}=\delta_{\mathrm{PEM},0}\sin(\omega t)]$.

In the absence of dichroism, the signal received at the detector is

$$I_{\mathrm{B}}=\frac{I_0}{2}[1+\cos(\delta_{\mathrm{PEM}})\sin(2\chi)\sin(\delta) - \sin(\delta_{\mathrm{PEM}})\cos(2\chi)\sin(\delta)]. \quad (3)$$

Here I_0 is the intensity transmitted by the first polarizer. Fourier expansion of $\sin(\delta_{\mathrm{PEM}})$ and $\cos(\delta_{\mathrm{PEM}})$ leads to an infinite series containing a dc term, I_{dc}, and harmonics of ω ($I_\omega, I_{2\omega}, I_{3\omega}$, etc.). By detecting one even and one odd harmonic (I_ω and $I_{2\omega}$) using the lock-in amplifiers and normalizing them with the signal from the low pass filter (I_{dc}), two equations which are independent of I_0 can be obtained.

$$R_\omega \equiv \frac{I_\omega}{I_{\mathrm{dc}}} = -2J_1(\delta_{\mathrm{PEM},0})\cos(2\chi)\sin(\delta), \quad (4)$$

$$R_{2\omega} \equiv \frac{I_{2\omega}}{I_{\mathrm{dc}}} = -2J_2(\delta_{\mathrm{PEM},0})\sin(2\chi)\sin(\delta), \quad (5)$$

where $J_1(\delta_{\mathrm{PEM},0})$ and $J_2(\delta_{\mathrm{PEM},0})$ are calibration constants whose magnitudes are determined experimentally using optical elements with known retardation.

Dichroism. If the sample displays dichroism and birefringence, Eq. (3) contains additional contributions and the harmonics I_ω and $I_{2\omega}$ are complex functions of retardation and extinction.[45] However, direct measurement of dichroism in the turbulent flow will demonstrate its magnitude to be small relative to that of the birefringence, as discussed subsequently. Dichroism measurements were accomplished with the configuration for birefringence less the circular polarizer $[LP_{@90°}PEM_{@45°}Q_{@0°}S'\delta''@\chi''^{°}]$.[45] For dichroism, the analogs of Eq. (4) and (5) then are

$$R''_\omega \equiv \frac{I_\omega}{I_{\mathrm{dc}}} = -2J_1(\delta_{\mathrm{PEM},0})\sin(2\chi'')\tanh(\delta''), \quad (6)$$

$$R''_\omega \equiv \frac{I_{2\omega}}{I_{\mathrm{dc}}} = -2J_2(\delta_{\mathrm{PEM},0})\cos(2\chi'')\tanh(\delta''). \quad (7)$$

Here S'' represents a polymer sample with dichroism extinction δ'' and dichroism orientation angle χ''. The extinction δ'' can be expressed as $\delta''=\Delta n''(2\pi d)/\lambda$, where $\Delta n''$ is the sample dichroism. Note that the signal from the dichroism optical train is independent of birefringence.

Turbidity. The dc signal from the low pass filter of the birefringence optical train represents the intensity of light propagated through the channel. Attenuation of this quantity measures the scattering and absorption of light by the injected polymers. The magnitude of attenuation provides an indirect characterization of the structure of polymers in the channel, since polymer agglomerates scatter light to a greater degree than single polymer molecules.

In a single-scattering approximation, the attenuation of monochromatic light is quantified by

$$I_{\mathrm{dc}} = I_{\mathrm{dc},0}\exp(-\nu d), \quad (8)$$

where d is the path length or the length of the channel in the neutral direction and v is Beer's law coefficient or the turbidity. This coefficient is independent of path length.

For birefringence, dichroism, and turbidity measurements, signals from the low-pass filter and lock-in amplifiers were acquired and analyzed using National Instruments' [Austin, TX] data acquisition system and LabView software. For experiments, polymer injection was performed for intervals that varied from 30 to 120 s. We observed acquired signals reached steady state within ten seconds. During this steady-state period, mean values of I_{dc}, I_ω, and $I_{2\omega}$ were computed by signal averaging. I_{dc} signal throughout inception, duration, and cessation of polymer injection is shown in Fig. 4. Measurements were acquired at a number of spatial positions along the gradient direction of the flow by traversing the entire optical system along the width of the channel.

4. Flow visualization apparatus

The evolution of the flow and the mixing taking place between the polymer solution and the channel flow was visualized by marking the injected polymer solution with fluorescein sodium salt, a water-soluble fluorescent dye. This technique is called laser induced fluorescence. The dye concentration was below 1 ppm and therefore does not significantly change the density of the fluid. A two-dimensional

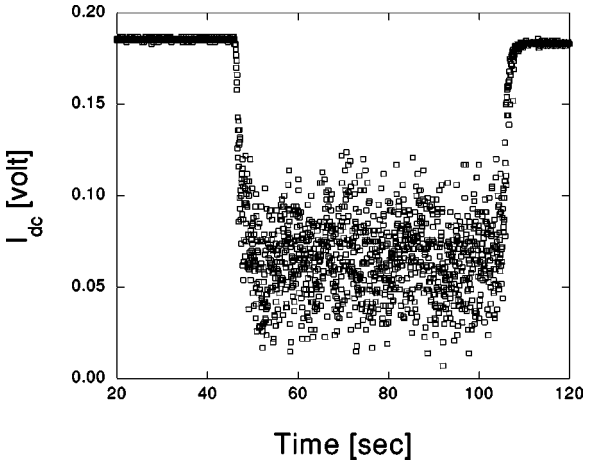

FIG. 4. Transient dc signal representing the intensity or transmittance of light beam through the channel at 29.98 mm from the wall ($\mathrm{Re}=5.2\times10^4$; $C_h=6.8$ ppm, and $C_i=10\,000$ ppm).

laser sheet of 1 mm thickness, oriented vertically (that is, in the plane define by the x and z axes), and centered at half-width of the channel was formed by using a cylindrical lens and a 2 W Lexar argon-ion laser. As the flouresecent dye passed through the laser sheet, the emitted light yieded a view of the dye concentration distribution in the plane of the laser sheet. A black and white 1000×1000 pixels Kodak Megaplus ES 1.0 charge-coupled device camera connected to a Matrox frame grabber was used.

C. Polymer solution preparation and experimental procedures

In this study a nonionic polyacrylamide (Hyperfloc NF301, Hychem Inc., Tampa, FL) is used as drag reducing agent. The weight average M_W molar mass, and z average radius of gyration ($R_{g,z}$) of this polydisperse polymer was measured by multiangle laser light scattering (Dawn EOS, Wyatt Technologies). The polymer sample was dissolved in degassed and filtered 0.1 M $NaNO_3$ aqueous buffer at concentrations of approximately 100 ppm. The stock solution was then diluted to six different concentrations ($\sim10-100$ ppm). These dilute solutions were then prefiltered (1.5 μm pore size), injected and the resultant scattering intensity measured in the angular range 26°–121°. A Berry formalism with a quadratic angular dependence was used to fit the scattered intensities at various concentrations and there by obtain M_W and $R_{g,z}$. By this method it was determined that for the polymer used in this study. $M_W=7.5\times10^6$ g/mole and $R_{g,z}=170$ nm.

The preparation of the aqueous solution follows a similar procedure to that of Koskie and Tiederman.[46] After combining the granular plymer, isopropyl alcohol, and water the solution requires both long-term hydration and gentle mixing. The process needs to provide enough agitation to avoid clumping without causing shear degradation of the polymer solution. A Bellco rolling apparatus was selsected to perform this taks. A comprehensive study to assess consistency of the polymer solution preparation procedures was performed and further details can be found in Ref. 47.

The polymer solution is injected through the slots in the channel walls for a short period of time. The time during which injection is maintained is determined by ensuring that no buildup on the concentration of effective polymers in the circulating solution takes place. That is, that the pressure at the channel test section remains constant in time ensuring that drag reduction remains also constant in time. After that time the polymer injection is topped and the circulating solution is run through the channel until the polymers are completely degraded. At that time injection and measurements are restarted. In this experiment the instataneous pressure at the test section is constant for a period of at least 10 min translating into constant drag reduction within ±0.03% during the same interval. After this period, injection is stopped and water recirculated for a period of another 10 min at maximum speed to fully degrade the polymer and recover the same pressure at the test section as that measured for water conditions. The overall change in flow rate corresponding to the maximum injection rate used in this study is less than 0.3%. Experiments were also conducted to assess the impact of the injection system on the flow at the test section. The experiments consisted of documenting the mean velocity and turbulence characteristics of the flow when water was injected, and comparing these results to the water data without injection. The latter results are reported and discussed in Sec. III B 1.

The measurements reported in this study were made at a Reynolds number equal to 5.6×10^4 based on the channel width and the centerline velocity. During the experiments the temperature was held constant at 22 ± 1 °C, which translates into a kinematic viscosity of $9.58\pm0.22\times10^{-7}$ m^2/s. The channel refrence velocity was monitored continuously with a GF-Signet 5100 flowmeter. The pressure taps were connectd to a W0602/IP-24T Scanivalve and Digi-Key 287-1027-ND temperatue compensated pressure sensor, with ±4 in H_2O range and a Pentium II PC was used to collect and process the signals.

III. RESULTS

A. Water flow

Measurements of the water flow, without injection, were initially made to validate the setup and instrumentation, to further corroborate the establishment of a fully developed flow at the test section and to be used as baseline measurements for comparison with the corresponding polymer flows. In the coordinate system (x,y) used in this paper, the x axis represents the streamwise direction and the y axis the direction normal to the wall. The corresponding mean and fluctuating components of the velocity are denoted (U,V) and (u,v), respectively. Symmetry of the flow with respect to the channel centerline was verified by measuring profiles of velocity and turbulence quantities all across the width of the channel. In this study the results corresponding to only one-half of the channel are presented.

For a Reynolds number of 5.6×10^4 based on the centerline velocity U_c and the channel width $2b$, the shear velocity u_τ [defined as $(\tau_w/\rho)^{1/2}$, where τ_w is the wall shear stress and ρ is the density of water] is 0.038 m/s. This corresponds to a

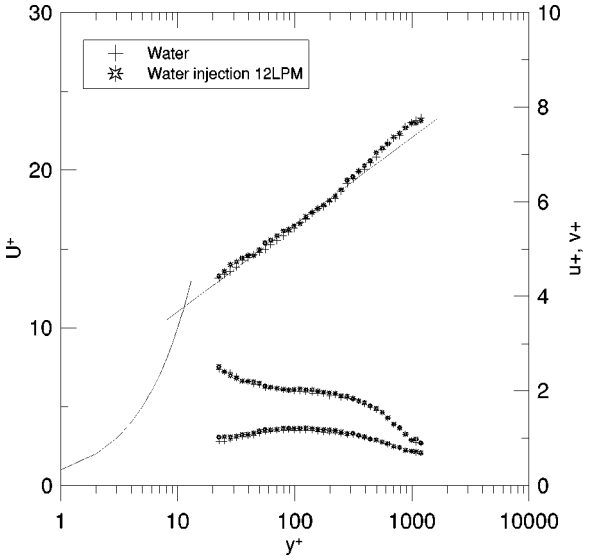

FIG. 5. Mean streamwise velocity and root mean square of the streamwise and normal velocity fluctuations for flow with water injection.

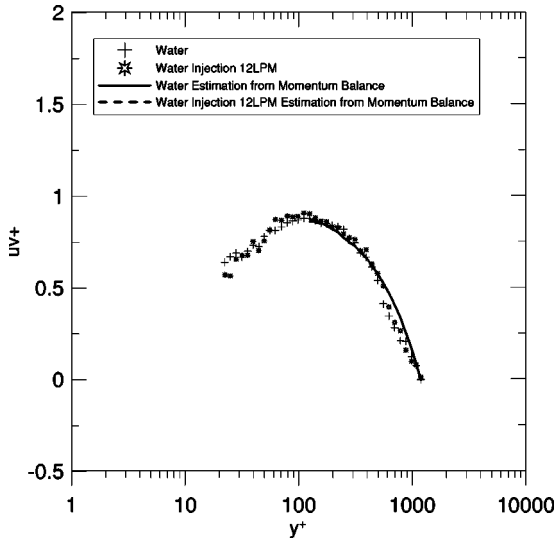

FIG. 6. Turbulent Reynolds stress for flow with water injection.

strain rate of 1508 s^{-1} at the wall, a viscous length of 25.2 μm, and $y^+=1190$ at the channel centerline. The shear velocity was computed based on pressure drop measurements, since in fully developed channel flows the wall shear stress is proportional to the pressure drop. It was also computed based on the linear variation of the total shear stress for a fully developed channel flow, which translates into the following expression of the shear velocity:

$$u_\tau^2 = \frac{(\nu dU/dy - \overline{uv})}{(1 - y/b)}. \tag{9}$$

The value of the shear velocity computed based on the pressure drop is within 5% of the shear velocity calculated based on expression (9).

Water injection experiments were also conducted to determine the effect of injection alone. Pressure drop measurements for both injection rates corresponding to both polymer injection concentrations reported in this study (i.e., 10 000 ppm and 1000 ppm) were taken when water was injected. The results show deviations from the water data well within 2%. LDV measurements of the flow with water injection corresponding to the higher injection flow rates (that is, 12 l/m ($=2\times10^{-4}$ m^3/s) for $C_i=1000$ ppm) were taken and the results compared with those of water.

Figure 5 shows the mean velocity along with the rms velocity fluctuations for water with and without water injection in inner normalized form, where $U^+=U/u_\tau$, $y^+=yu_\tau/\nu$, and ν represents the kinematic viscosity of water. The streamwise velocity component and corresponding rms show very minor differences with the flow without injection.

Figure 6 shows the comparisons of the Reynolds stress corresponding to water with and without injection. Also shown in the figure is the Reynolds stress profile obtained based on the momentum equation and the measured mean velocity profile as

$$\tau_w\left(1 - \frac{y}{b}\right) = \mu\frac{dU}{dy} - \rho\overline{uv}. \tag{10}$$

The agreement between the indirect measurements of the Reynolds stress via Eq. (10) and the direct LDV measurements is very good. This check provides a test of the accuracy of the direct measurements of the Reynolds stress. The determination of dU/dy is done by differentiating the experimental data directly and the results were checked versus that obtained from the best polynomial fit to the measured mean velocity (i.e., a 15th-order polynomial curve). The results agreed within 5% in the region $100<y^+<500$.

The errors due to the finite size of the measuring volume translate into uncertainties up to 3% in the region $50<y^+<1300$ and less than 15% in the rest of the channel. The contribution from electrical noise was estimated to be less than 5% in the region $50<y^+<1300$ and around 10% in the rest of the channel. These results are comparable to those of Warholic,[40] Warholic *et al.*,[18] and others.

B. Polymer flow

Experiments were conducted at the same Reynolds number of 5.6×10^4 with polymer injection from both vertical injection slots at the entrance of the channel. The injection concentration was deemed an important parameter whose effect on the flow had to be evaluated. In order to do so, experiments were conducted for the same homogeneous concentration at the test section but with different injection concentrations and injection flow rates. The results translated into important differences in drag reduction for certain levels of injection concentration. In this section the data resulting from mean and turbulence measurements of the polymer flow for a test section homogeneous concentration of 14 ppm but injection concentrations of 10 000 ppm and 1000 ppm are reported and discussed. The drag reduction percentage, defined as $[100(\tau_{wN^-})\tau_w)/\tau_{wN}]$, where τ_{wN} represents the wall shear stress for the Newtonian flow, resulted in a drag

reduction level of 39% for the larger injection concentration, while for the lower injection concentration the drag reduction was 13%.

Measurements were conducted also for a test section homogeneous concentration of 7 ppm but are not reported here since the results are very similar to those found for 14 ppm. The levels of drag reduction for both injection concentrations (i.e., 1000 ppm and 10 000 ppm) are comparable for both test section concentrations (i.e., 7 ppm and 14 ppm). Some preliminary results for the 7 ppm case can be found in Ref. 48.

1. Mean and turbulence characteristics

The results for the mean velocity, rms velocity fluctuations, and Reynolds stress are presented next and compared to the results corresponding to the fully developed channel flow without polymer injection. All results are nondimensionalized by using the shear velocity corresponding to the fully developed flow without injection as the characteristic velocity, and the ratio of the kinematic viscosity of water to the water friction velocity as the characteristic length, unless otherwise specified.

Figures 7(a) and 7(b) show the dimensionless mean streamwise velocity profiles for both polymer flows and water. The nondimensionalization in Fig. 7(b) makes use of the shear velocity corresponding to each case (see Table I) instead of the one for the water flow for all the cases, which is shown in Fig. 7(a). With respect to the water flow the polymer flow near the wall is decelerated while the flow away from the wall is accelerated [Fig. 7(a)]. The thickness of the viscous sublayer increases, translating into smaller u_τ for the polymer flows, and consequently the logarithmic region is moved up [Fig. 7(b)]. While for the low injection concentration the logarithmic region experiences a shift upwards, for the high injection concentration the logarithmic region also changes slope. This is expected for large drag reduction percentages.[17,18] The latter results for the high injection concentration are however below the maximum drag reduction asymptote shown in Fig. 7(b) as a solid line. These trends are consistent with those observed in the past by other researchers.

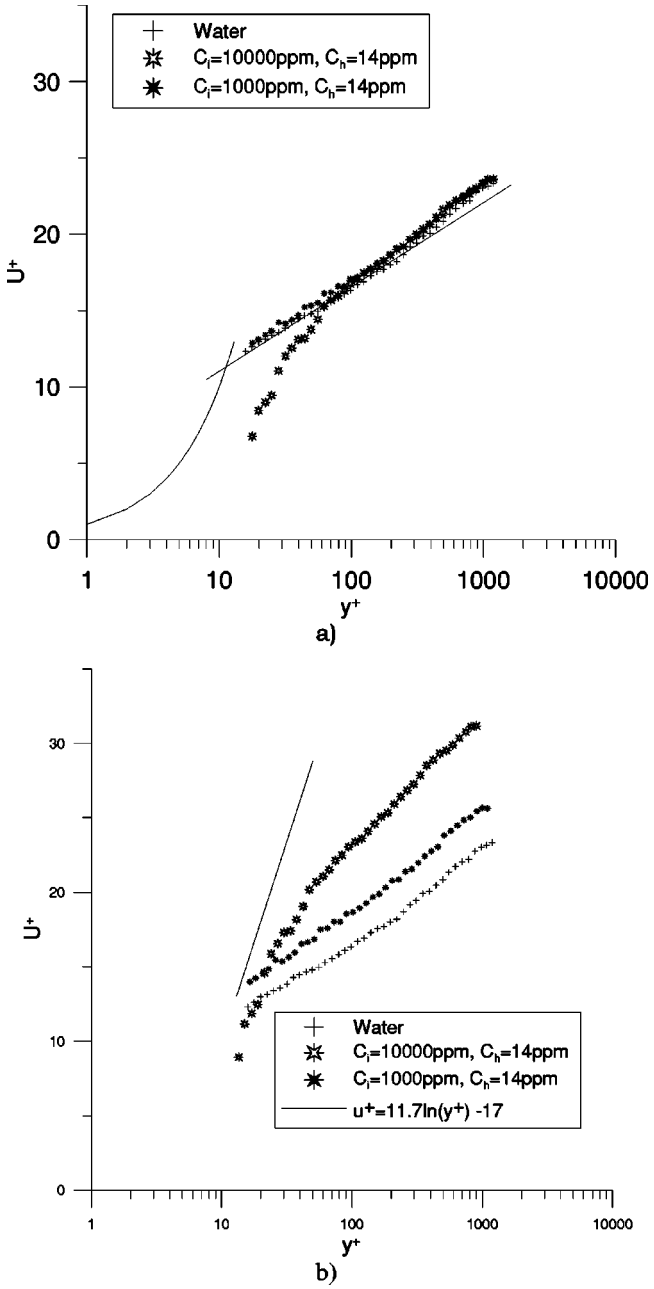

FIG. 7. Mean streamwise velocity for flow with polymer injection. (a) Polymer data were normalized by water u_τ; (b) polymer data were normalized by each polymer u_τ.

The distribution of the rms corresponding to the dimensionless streamwise velocity fluctuations is shown in Fig. 8. For both polymer flows the maximum u^+ is displaced away from the wall, consistent with a thicker viscous sublayer and a smaller shear velocity. The maximum corresponding to the low injection concentration case is higher than the maximum u^+ for water, while that corresponding to the high injection concentration case is roughly the same as that for water. While qualitatively the profile corresponding to the lower injection concentration looks very similar to that of water (both profiles agree in the region $y+>100$), the same cannot be said for the profile corresponding to the higher injection concentration which seems to be altered all throughout the half-width of the channel.

The rms corresponding to the dimensionless normal velocity fluctuation data, shown in Fig. 9, shows a decrease in the near wall region with polymer injection. While the changes are small for the polymer solution with low drag reduction (values become comparable to those of water for $y+>100$), the measurements of v^+ are significantly lower for the larger injection concentration all across the channel.

The profile corresponding to the turbulent Reynolds stress is shown in Fig. 10. It reveals a systematic decrease all across the channel up to $y^+\sim 800$ and $y^+\sim 200$ for the higher and lower injection concentrations respectively where the data becomes comparable to that of water. The magnitude and location of the maximum in $-uv^+$ change with polymer injection concentration and homogenous concentration. For the larger injection concentration the maximum is reduced by more than 40% and is located about 150 viscous lengths

TABLE I. Main flow parameters. Re_τ is based on u_τ, half channel width, and water viscosity at 22 °C, while Re is based on centerline velocity, channel width, and water viscosity at 22 C.

Flow type	Water	Polymer	Polymer
Water temperature (°C)	22±1	22±1	22±1
Injection concentration C_i (ppm)	⋯	10 000	1 000
Mixed concentration C_h (ppm)	⋯	14	14
Percentage of drag reduction	⋯	39.0	13.1
Centerline velocity U_C (m/s)	0.892	0.884	0.897
u_τ (m/s)	0.038	0.029	0.035
y (mm) at $y^+=1$	0.025	0.033	0.027
Re	55 869	55 369	56 154
Re_τ	1 190	908	1 096

from the wall. The smaller injection concentration translates into a reduction of the peak turbulent Reynolds stress of 10% located at $y^+=160$.

The reduction of the Reynolds stress in the buffer region indicates that polymers influence the turbulent momentum transfer. However, this reduction can be due to lower turbulence intensities as shown for v^+ in Fig. 9, and/or to a decorrelation between the streamwise and normal velocity fluctuations. Figure 11 shows the covariance of these fluctuations or the Reynolds shear stress correlation coefficient defined as

$$C_{uv} = \frac{-\overline{uv}}{(u^2v^2)^{1/2}}. \tag{11}$$

The results shown in Fig. 11 include water and polymer data. The water data show a maximum of 0.43 at $y^+ \sim 200$. This result seems to be in agreement with Kim *et al.*.[49] The polymer data show a reduction of the correlation coefficient. This result indicates that the reduction of the shear stress shown in Fig. 10 is in part explained by reductions in the contributions of the velocity fluctuations to the momentum transport in comparison to water flow. The streamwise and

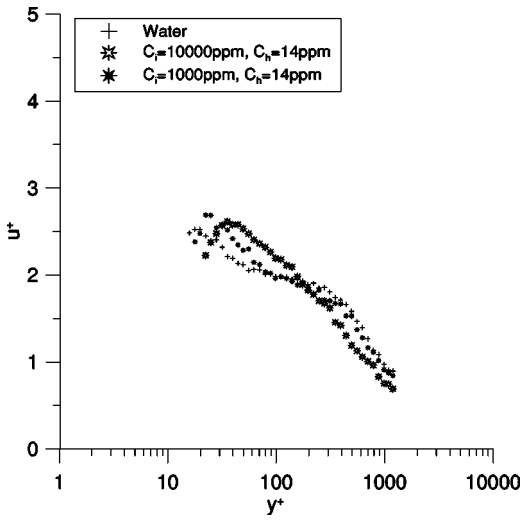

FIG. 8. Root mean square of the streamwise velocity fluctuation for flow with polymer injection.

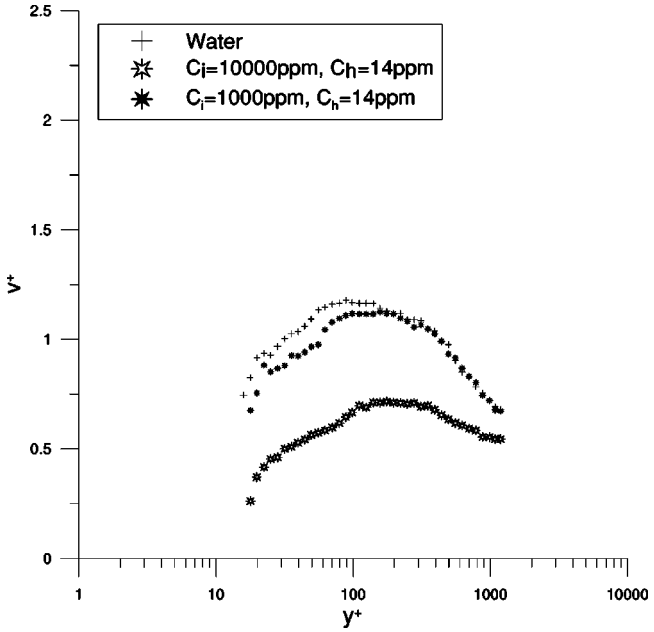

FIG. 9. Root mean square of the normal velocity fluctuation for flow with polymer injection.

normal velocity fluctuations become more decorrelated the higher the injection concentration is (for the same concentration at the test section).

2. Flow visualization results

The data discussed in the preceding section indicate that while the same homogeneous concentration of 14 ppm was targeted at the test section and both injected solutions (1000 ppm and 10 000 ppm) seemed homogeneously mixed there are obvious differences in their drag reducing abilities. To better understand the differences between the two poly-

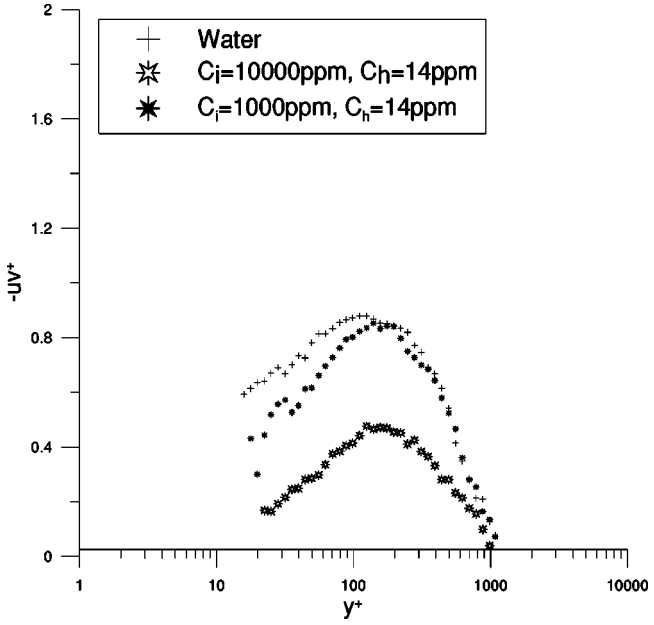

FIG. 10. Turbulent Reynolds stress for flow with polymer injection.

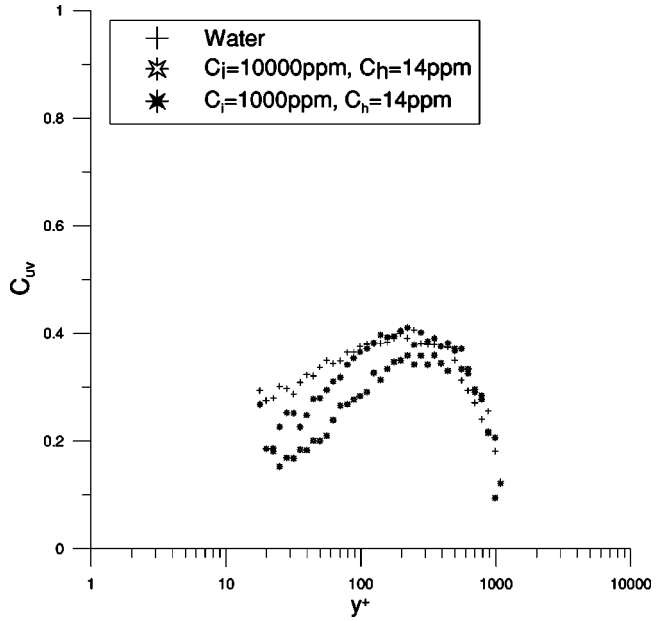

FIG. 11. Reynolds stress correlation coefficient for flow with polymer injection.

mer flows, flow visualization experiments are conducted and birefringence measurements taken. The latter will be discussed in the next section.

Laser induced fluorescence is done by visualizing a mixture of the polymer solution with fluorescent dye and illuminating it with a planar laser sheet. The camera is located 76 channel widths downstream from the injection slot. The size of the window is set at 10.2 cm $\times$ 7.6 cm with a corresponding resolution of 400 pixels per inch (63.5 μm/pixel). The laser sheet is vertical and located half-width in the channel at the test section. Visualizations are performed for 10 000 and 1000 ppm injection concentrations and a corresponding concentration at the test section of 14 ppm.

No indication of any appreciable differences with respect to the flow with water injection is observed for the polymer flow with low injection concentration. However, for the polymer flow with the higher injection concentration (i.e., 10 000 ppm) the presence of macromolecular polymer structures seems to be revealed as it is shown in Fig. 12(a). The flow direction in the picture is from left to right, and the exposure time is 20 ms. The results shown in Fig. 12(a) correspond to the visualization of the flow 15 s after injection of the polymer solution. At that same time visualization of the flow at the test section at about $y^+=100$, shown in Fig. 12(b), shows less and smaller structures in the near wall region than in the centerline. This result was shown to be consistent at other times after injection when the flow was visualized at the centerline and $y^+=100$ at the test section. Furthermore, flow visualizations were conducted close to the injection slot and structures seem evident right after polymer injection, which will seem to indicate that they were, in part at least, being formed in the process of injection.

These results along with the fact that a considerable increase of drag reduction is observed for larger injection concentration at a flow rate set to obtain identical homogeneous

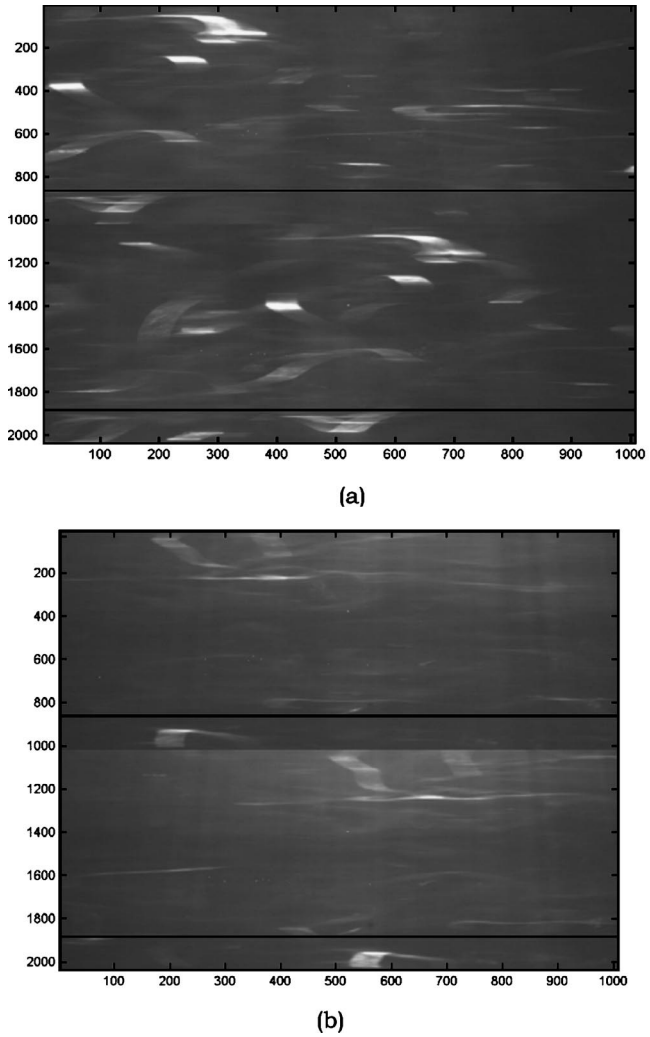

FIG. 12. Visualization of turbulent channel flow with $C_i=10\,000$ ppm and $C_h=14$ ppm (a) at the centerline of the test section; (b) at $y^+=100$.

concentrations at the test section, appear to agree with the conclusions reached by Warholic *et al.*[18] regarding polymer effectiveness being associated with the formation of polymer structures. The present visualizations though, are inconclusive as to where the polymer structures are located within the flow. To better address this point birefringence measurements were taken and are discussed in the following section.

3. Birefringence results

Figures 13 and 14 report the results of birefringence and turbidity measurements, respectively, at $\mathrm{Re}=5.2\times10^4$. Although the homogeneous (fully mixed) concentration is fixed at $C_h=14$ ppm, the polymer injection concentration was varied between 1000 ppm and 10 000 ppm to probe the effect of this variable on optical properties. The drag reduction percentages corresponding to $C_i=1000$ ppm, 3000 ppm, 5000 ppm, 8000 ppm, and 10 000 ppm are 13%, 26.3%, 28.3%, 38.4%, and 39%, respectively.

Each of these measures of polymer optical properties suggests a strong effect of polymer injection concentration. Birefringence and turbidity each increase with increasing

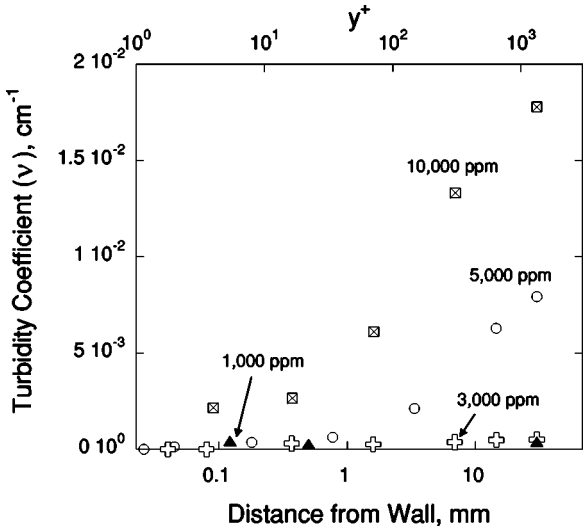

FIG. 13. Turbidity coefficient distribution across the channel for different injection concentrations and $C_h = 14$ ppm.

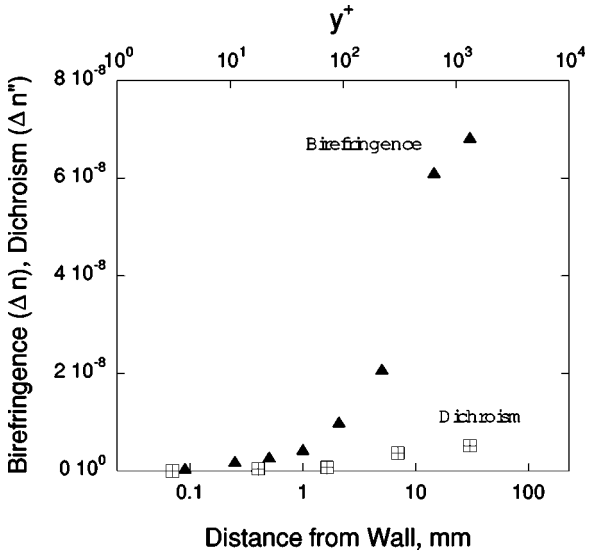

FIG. 15. Comparison of birefringence and dichroism across the channel for $C_i = 10\,000$ ppm and $C_h = 14$ ppm.

polymer injection concentration. Moreover, interestingly, the optical effects are greatest at the centerline of the flow, at the maximum distance from the wall.

Figure 15 gauges the extent to which the measurement of birefringence, characterized by means of Eqs. (4) and (5), is possibly complicated by the existence of dichroism. At 10 000 ppm polymer injection concentration birefringence is much greater than dichroism. Thus, it can be concluded that the application of Eqs. (4) and (5) to extract birefringence is appropriate, and that Fig. 14 is correctly reported as birefringence.

Figure 16 addresses the extent to which the turbidity measured during polymer injection is a flow-induced phenomenon, or if microscopic structures giving rise to significant scattering might already be present in the concentrated polymer solution prior to injection. Turbidity measurements were conducted under quiescent conditions at a range of concentrations. Figure 16 shows that at low polymer concentrations the turbidity coefficient ν exhibits a linear relationship with concentration. In this regime, turbidity results from scattering of light by individual macromolecules with negligible intermolecular interaction. At higher concentration when intermolecular interactions are significant, the trend deviates from linearity. It is instructive to compare the absolute magnitude of the turbidity coefficients in the quiescent measurements of Fig. 16, to the studies in the flow channel, which were reported in Fig. 13. The comparison demonstrates that the turbidity measured near the centerline for $C_i > 3000$ ppm and $C_h \sim 14$ ppm in Fig. 13 is orders of magnitude higher than found in the quiescent studies. The finding strongly indicates that the polymer concentrations at the centerline of the channel flow device are inhomogeneous for polymer injection concentrations $C_i > 3000$ ppm, and that the inhomogeneity is induced by flow in the injector or channel.

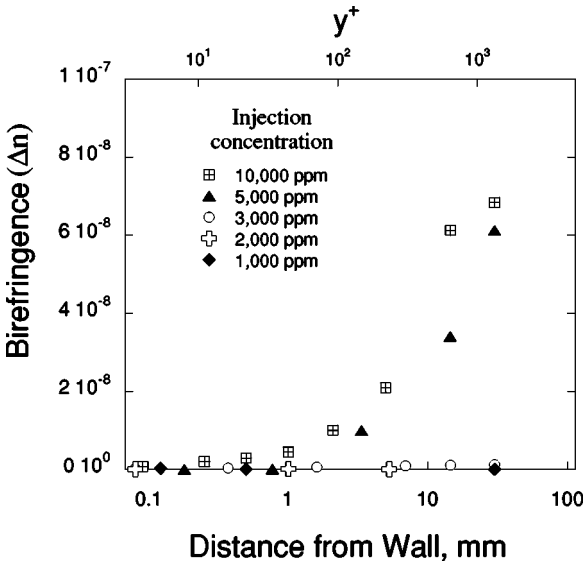

FIG. 14. Birefringence retardance distribution across the channel for different injection concentrations and $C_h = 14$ ppm.

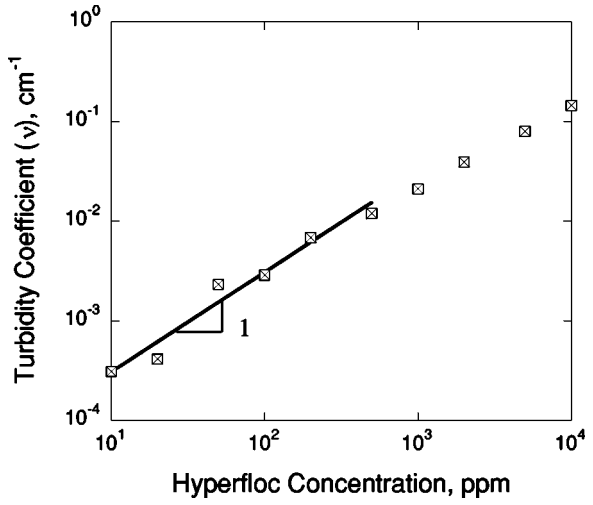

FIG. 16. Turbidity of quiescent Hyperfloc solutions at different concentrations.

IV. DISCUSSION

The results presented herein can be thought to have some similarities with those from heterogeneous drag reduction.[50,51,12] In those studies highly concentrated polymer solutions of long chain, high molecular weight polymer, are injected into the core region of a turbulent pipe or channel. In such cases and if the concentration is large enough ($c_i \geqslant 4000$ ppm) a single coherent thread is formed that preserves its identity for long distances after injection. In this study while the concentration of the injected solution, when heterogeneous drag reduction was achieved, was very large (10 000 ppm), it was injected in the near wall region at an angle of 25° to the wall with a slot 0.25 cm wide along both sides of the channel. Special attention was given to ensure, to the extent possible, that no appreciable polymer structures were present in the injected solution. Flow visualization results indicate that threadlike structures can be seen early on in the near wall region of the channel. Quick mixing takes place in the channel, and eventually the bulk of the larger threads is mostly located along the channel's centerline as shown by birefringence and turbidity measurements. These results indicate that the high shear that takes place in the injection system may trigger the formation of the polymer structures. Throughout the mixing that takes place in the channel prior to the test section, the threads near the wall are ejected towards the outer region of the boundary layer where the shear is less. From the centerline polymer is also being entrained toward the wall as shown by some of the past studies on heterogeneous drag reduction. Visually, the size of the structures in the near wall region seem to be smaller than those along the centerline, and their presence is highly intermittent. Birefringence measurements showed that injection concentrations larger than 3000 ppm are linked with the formation of macromolecular polymer structures by the time the polymer reaches the test section. No such appreciable structures were detected for lower concentrations. It should be emphasized once again that these experiments do not preclude the presence of small polymer structures for the case corresponding to the lowest injection concentrations ($c_i < 3000$ ppm), labeled as representative cases of homogeneous drag reduction. However, such structures, if they are present, would need to be much smaller than the wavelength of light, because no significant turbidity is measured for $c_i < 3000$ ppm.

A detailed comparison of the mean and turbulent flow characteristics for a test section concentration of 14 ppm under different conditions, homogeneous and heterogeneous drag reduction, was conducted. When macromolecular polymer structures were present in the flow the viscous sublayer was thickened and the rms values of the streamwise and normal velocity fluctuations reduced, as well as the Reynolds stress. The results showed an increase in drag reduction of three times for the heterogeneous case versus the homogeneous case. The mechanism by which changes in polymer concentration at the centerline affect the behavior in the buffer layer is unknown and warrants future investigation. In any case the large increase in drag reduction induced by the presence of polymer structures indicates that special care should be taken into optimizing the design of the injection system to promote concentration inhomogeneity since it can translate into substantial changes in drag reduction. This is particularly important in practical applications where the polymer solution needs to be injected. Similarly, it will seem that the time spent into preparing well-mixed homogeneous solutions, as done in this study, is not fully justified, indeed the ability of polymers to aggregate or entangle might be an important asset in drag reduction. The recent study of Vlachogiannis and Hanratty[29] corroborates this conclusion for turbulent flow over a wavy wall with an injected solution of HPAM. Small injection concentrations ($c_i \geqslant 500$ ppm) were used by comparison to this study or others in the past where heterogeneous drag reduction was achieved. In their study, however, polymer structures were already present in the solution prior to injection. Our work suggests that even initially homogeneous polymer solutions can yield improved drag reducing capability if inhomegenity is induced in them.

ACKNOWLEDGMENTS

This work was supported by the Defense Advance Research Projects Agency (DARPA) under Grant No. MDA972-01-1-0014, as part of the Friction Drag Reduction Program. A significant portion of the equipment used in this study was acquired under Office of Naval Research, Defense University Research Instrumentation Program, Grant No. N00014-99-1-0662 with cost sharing by the University of Michigan. This support is gratefully acknowledged. The authors wish to thank the help provided by Dr. Kathleen Tacina, now at NASA Glenn Research Center (Cleveland, OH), in the design and construction of the water channel, as well as with the setup of the experimental instrumentation in the early stages of this study. The help of S. A. Vanapalli performing the GPC characterization of the polymer solutions is also greatly appreciated.

[1] B. A. Toms, "Some observations on the flow of linear polymer solutions through straight tubes at large Reynolds numbers," in *Proceedings of the First International Congress in Rheology* (Academic, New York, 1948).
[2] R. H. J. Sellin, J. W. Hoyt, J. Pollert, and O. Scrivener, "The effect of drag-reducing additives on fluid flows and their industrial applications part 1: Present applications and future proposals," J. Hydraul. Res. **20**, 235 (1982).
[3] E. H. Dunlop and L. R. Cox, "Influence of molecular aggregates on drag reduction," Phys. Fluids **20**, S203 (1977).
[4] J. W. Hoyt, Drag reduction, *Encyclopedia of Polymer Science and Engineering*, Vol. 5, edited by H. F. Mark *et al.* (Wiley, New York, 1986), p. 129.
[5] M. J. Richardson, "The direct observation of polymer molecules and determination of their molecular weight," Proc. R. Soc. London, Ser. A **279**, 50 (1964).
[6] M. W. Liberatore, E. J. Pollauf, and A. J. McHugh, "Shear-induced structure formation in solutions of drag reducing polymers," J. Non-Newtonian Fluid Mech. **113**, 193 (2003).
[7] R. Boyadjian, G. Seytre, P. Berticat, and G. Vallet, "Physicochemical characterization of polyacrylamides used as flocculating agents. 1. Study in solution," Eur. Polym. J. **12**, 40 (1976).
[8] R. Boyadjian, G. Seytre, D. Sage, and P. Berticat, "Physicochemical characterization of polyacrylamides used as flocculating agents. 2. Insoluble fractions," Eur. Polym. J. **12**, 409 (1976).
[9] J. L. Lumley, "Drag reduction in two phase and polymer flows," Phys. Fluids **20**, S64 (1977).
[10] P. G. DeGennes, "Towards a scaling theory of drag reduction," Physica A **140**, 9 (1986).

[11]B. O'Shaughnessy, C. Durning, and M. Tabor, "Polymer deformation in strong high-frequency flows," J. Chem. Phys. **92**, 2637 (1990).
[12]H. W. Bewersdorff, A. Gyr, K. Hoyer, and A. Tsinober, "An investigation of possible mechanisms of heterogeneous drag reduction in pipe and channel flows," Rheol. Acta **32**, 140 (1993).
[13]M. M. Rieschman and W. G. Tiederman, "Laser-Doppler anemometer measurements in drag-reducing channel flows," J. Fluid Mech. **70**, 369 (1975).
[14]T. Wei, and W. W. Willmarth, "Modifying turbulent structure with drag-reducing polymer additives in turbulent channel flows," J. Fluid Mech. **245**, 619 (1992).
[15]J. M. M. Den Toonder, M. A. Hulsen, G. D. C. Kuiken, and F. T. M. Nieuwstadt, "Drag reduction by polymer additives in a turbulent pipe flow: Laboratory and numerical experiments," J. Fluid Mech. **337**, 193 (1997).
[16]P. K. Ptasinski, F. T. M. Nieuwstadt, B. H. A. A. Van Den Brule, and M. A. Hulsen, "Experiments in turbulent pipe flow with polymer additives at maximum drag reduction," Flow, Turbul. Combust. **66**, 159 (2001).
[17]B. Gampert and A. Delgado, "Laser-Doppler anemometer measurements in turbulent flow of viscoelastic fluids," in *Proceeding of the International Symposium on Laser Anemometry* (ASME, New York, 1985).
[18]M. D. Warholic, H. Massah, and T. J. Hanratty, "Influence of drag-reducing polymers on turbulence: Effects of Reynolds number, concentration and mixing," Exp. Fluids **27**, 461 (1999).
[19]G. L. Donohue, W. G. Tiederman, and M. M. Reischman, "Flow visualization of the near-wall region in a drag-reducing channel flow," J. Fluid Mech. **56**, 559 (1972).
[20]O. K. Oldaker and W. J. Tiederman, "Spatial structure of the viscous sublayer in drag-reducing channel flow," Phys. Fluids **20**, S133 (1977).
[21]B. U. Achia and D. W. Thompson, "Structure of the turbulent boundary in drag-reducing pipe flow," J. Fluid Mech. **81**, 439 (1977).
[22]W. G. Tiederman, T. S. Luchich, and D. G. Bogard, "Wall layer structure and drag reduction," J. Fluid Mech. **156**, 419 (1985).
[23]T. S. Luchik and W. G. Tiederman, "Turbulent structure in low-concentration drag-reducing channel flows," J. Fluid Mech. **190**, 241 (1988).
[24]B. Gampert, T. Braemer, T. Eich, and T. Dietmann, "Some experimental results on laser Doppler velocimetry (LDV) and birefringence (FIB) studies of non-Newtonian fluids flow through rectangular channels," in *Proceedings of the Fourth ASME/JSME Joint Fluids Engineering Conference*, Hawaii (ASME, New York, 2003).
[25]R. Sureshkumar, A. N. Beris, and R. A. Handler, "Direct numerical simulation of the turbulent channel flow of a polymer solution," Phys. Fluids **9**, 743 (1997).
[26]C. D. Dimitropoulos, R. Sureshkumar, A. N. Beris, and R. A. Handler, "Budgets of Reynolds stress, kinetic energy and streamwise entrophy in viscoelastic turbulent channel flow," Phys. Fluids **13**, 1016 (2001).
[27]R. Benzi, E. De Angelis, R. Govindarajan, and I. Procaccia, "Shell model for drag reduction with polymer additives in homogeneous turbulence," Phys. Rev. E **68**, 016308 (2003).
[28]E. De Angelis, C. M. Casciola, V. S. L'vov, and R. Piva, "Drag reduction by polymers in turbulent channel flows: Energy redistribution between invariant empirical modes," Phys. Rev. E **67**, 056312 (2003).
[29]M. Vlachogiannis and T. J. Hanratty, "Influence of wavy structured surfaces and polymer aggregation on drag reduction," Exp. Fluids **36**, 685 (2004).
[30]M. Vlachogiannis, M. W. Liberatore, A. J. McHugh, and T. J. Hanratty, "Effectiveness of drag-reducing polymers: Relation to molecular weight distribution and structuring," Phys. Fluids **15**, 3786 (2003).
[31]R. B. Dean, "Reynolds number dependence of skin friction and other bulk flow variables in two-dimensional rectangular duct flow," J. Fluids Eng. **100**, 215 (1978).
[32]G. Comte-Bellot, "Ecoulement turbulent entre deux parois paralleles," Publications Scientifiques et Techniques du Ministere de l'Air, No. 419, 1965.
[33]T. Wei, "Reynolds number effects on the small scale structure of a turbulent channel flow," Ph.D. thesis, Department of Aerospace Engineering, The University of Michigan, 1987.
[34]J. S. Velazquez, "Design, construction, and use of a high-resolution, two-component LDA," Ph.D. thesis, Department of Aerospace Engineering, The University of Michigan (1983).
[35]D. T. Walker, W. G. Tiederman, and T. S. Luchik, "Optimization of the injection process for drag reducing additives," Exp. Fluids **4**, 114 (1986).
[36]T. Wei and W. W. Willmarth, "Reynolds-number effects on the structure of a turbulent channel flow," J. Fluid Mech. **204**, 57 (1989).
[37]S. Kang, B. Patil, and R. P. Roy, "Effects of coincidence window and measuring volume size on laser Doppler velocimetry measurement of turbulence," Exp. Fluids **30**, 365 (2001).
[38]M. A. Niderschulte, R. J. Adrian, and T. J. Hanratty, "Measurements of turbulent flow in a channel at low Reynolds numbers," Exp. Fluids **8**, 222 (1990).
[39]A. Günter, D. V. Papavassiliou, M. D. Warholic, and T. J. Hanratty, "Turbulent flow in a channel at a low Reynolds number," Exp. Fluids **16**, 36 (1998).
[40]M. D. Warholic, "Reynolds number effects on the velocity statistics in a turbulent channel flow," M.S. thesis, Department of Chemical Engineering, University of Illinois at Urbana-Champaign, 1995.
[41]A. V. Johansson and P. H. Alfredsson, "Effects of imperfect spatial resolution on measurements of wall-bounded turbulent shear flows," J. Fluid Mech. **137**, 409 (1983).
[42]R. F. Blackwelder and J. H. Haritonidis, "Scaling of the bursting frequency in turbulent boundary layers," J. Fluid Mech. **132**, 87 (1983).
[43]T. S. Luchik and W. G. Tiederman, "Effect of spanwise probe volume length on laser velocimeter measurements in wall bounded turbulent flows," Exp. Fluids **3**, 339 (1986).
[44]F. Durst, J. Jovanovic, and J. Sender, "LDA measurement in the near-wall region of a turbulent pipe flow," J. Fluid Mech. **295**, 305 (1995).
[45]G. G. Fuller, *Optical Rheometry of Complex Fluids* (Oxford University Press, New York, 1995).
[46]J. E. Koskie and W. G. Tiederman, "Turbulence structure and polymer drag reduction in adverse pressure gradient boundary layers," Technical Report PME-FM-91-3, Purdue University, West Lafayette, IN, 1991.
[47]R. Sun-Chee-Fore, J. Miller, K. Tacina, and A. I. Sirviente, "Effect of degradation on polymer drag reduction in a turbulent channel flow," Bull. Am. Phys. Soc. **47**, 90 (2002).
[48]X. Shen, K. Kim, J. Miller, R. Sun-Chee-Fore, and A. I. Sirviente, "Experimental study of polymer drag reduction in a turbulent channel flow," in *Proceedings of the Fourth ASME JSME Joint Fluids Engineering Conference*, Hawaii (ASME, New York, 2003).
[49]J. Kim, P. Moin, and R. Moser, "Turbulence statistics in fully developed channel flow at low Reynolds number," J. Fluid Mech. **177**, 133 (1987).
[50]J. Vleggaar and M. Tels, "Drag reduction by polymer threads," Chem. Eng. Sci. **28**, 965 (1973).
[51]R. E. Smith and W. G. Tierderman, "The mechanism of polymer thread drag reduction," Rheol. Acta **30**, 103 (1991).